Coherence measure in Hamiltonian systems with many degrees of freedom

Maira D'Alessandro
Physics Department, University of Perugia, Via A. Pascoli 1, 06100 Perugia, Italy

Andrea D'Aquino
Physics Department, ''La Sapienza'' University, Piazzale A. Moro 2, 00185 Rome, Italy

Alexander Tenenbaum*
Unità di Roma 1, Istituto Nazionale di Fisica della Materia and Physics Department, ''La Sapienza'' University, Piazzale A. Moro 2, 00185 Rome, Italy

(Received 4 April 2000)

We study the phase space region of two- and three-dimensional lattices where a transition from chaotic to ordered dynamics takes place when the energy is lowered. In this region we find coexistence of degrees of freedom (DOF's), endowed with different levels of chaos. The analysis of this complex dynamical pattern requires the introduction of diagnostic tools suitable for a characterization of single DOF's: coherence angles and coherence times. We find that the coherence times—which give a measure of the time each DOF needs to relax to equilibrium—are roughly proportional to the inverse of the specific energy. This may be useful to evaluate the reliability of statistical results obtained in computer experiments performed on condensed matter systems at low energy.

PACS number(s): 05.45.−a, 63.22.+m, 63.70.+h

I. INTRODUCTION

The phase space of an integrable Hamiltonian system is foliated in invariant tori; an orbit starting at a point on a torus remains forever on this torus, without diffusing on the hypersurface of constant energy. Up to the early 1950s it was commonly assumed that an arbitrarily small perturbation of the integrable Hamiltonian would destroy the invariant tori, making the sistem quasiergodic. This belief rested on a theorem by Poincaré [1], resumed and completed by Fermi [2]. But in 1954 a famous computer experiment on a one-dimensional (1D) lattice, by Fermi, Pasta, and Ulam (FPU) [3], showed that a condensed matter system modeled by a harmonic Hamiltonian perturbed by nonlinear terms may well not approach equilibrium, at odds with the traditional expectation. In later years a lively discussion has developed, which still goes on, concerning the relevance of those findings—and of many others similar in more recent years—to the foundations of classical statistical mechanics. The existence of partially ordered motions in regions of the phase space of positive measure, which emerged from the FPU experiment, and was explained by the Kolmogorov-Arnold-Moser (KAM) theorem [4], questioned the equivalence of time averages and averages performed on a microcanonical ensemble. Numerical estimates showed that the region of ordered motions is of physical relevance, but they could not answer the question of whether the measure of this region would remain significant in the thermodynamic limit. While some analytical evaluations gave a negative answer to this last question, results of computer experiments seem to point in the opposite direction [5].

These questions are of specific relevance for condensed matter systems. At high temperature the dynamics of the particles is determined to a great extent by the repulsive hard core of the interaction potential, making them behave similarly to hard spheres, which is a system believed to be quasiergodic. At low temperature, a solid may be represented by a harmonic Hamiltonian, perturbed by nonlinear terms; such a Hamiltonian is nearly integrable, and thus of the type required by the KAM theorem for the existence of ordered motions. These simple euristic arguments show that when the energy of a generic condensed system is lowered, the latter must undergo a transition from a chaotic, quasiergodic state, to an ordered, nearly integrable one [6]. The energy around which this transition should occur varies from system to system, and for most systems can be determined only numerically; moreover, the dependence of this threshold on the number of degrees of freedom (DOF's) remains an open question.

In 1977 a theorem by Nekhoroshev [7] introduced a new point of view in the problem, giving it a different aspect. He showed that even in the phase space region characterized by a quasiergodic behavior, a fraction of the dynamical DOF's of the system behave in a quasiintegrable way over times which may diverge for small nonlinearity. So another question was raised: provided the initial state of the system is in the quasiergodic region, how long should one follow the trajectory (in a real, or in a computer experiment) in order to be sure to gather a good statistical result, independent of the initial conditions?

In recent years these problems have been put in a comprehensive framework, through the concept of a strong stochasticity threshold (SST), a specific energy per DOF [5,8]. The phase space is separated by the SST in two regions: at energies higher than the SST, the system is characterized by a highly chaotic dynamics (Anosov-type diffusion); while at

*Author to whom correspondence should be addressed. Electronic address: tenenbaum@roma1.infn.it

energies lower than the SST, the dynamics is very weakly chaotic (Arnold-type diffusion). From this point of view, the question in analyzing the dynamics of a nonlinear system is not whether the system is chaotic or not, but the following one: how long does it take for the system to exhibit a chaotic behavior? As a matter of fact, this time may be so long that, for all practical purposes, the system may be seen as ordered [9]. A second question concerns the dependence of this time on the size of the system. The definition of a SST allows an analytical estimate of its dependence on the number of DOF's for the FPU system [5]. The estimate indicates that the SST should persist in the thermodynamic limit. This result does not obviously give an ultimate answer to the question—raised at the beginning of this section—concerning the relevance of an ordered dynamics for the thermodynamic properties of a system. One should note, however, that physics often deals with systems which are very small on a macroscopic scale, yet have a sufficiently large number of DOF's to be treated statistically (e.g., clusters of particles, and macromolecules). For these systems one can reasonably expect the macroscopic properties to be influenced by the presence of persistent ordered motions, in a physically relevant low energy range.

The Nekhoroshev theorem and the existence of the SST lead quite naturally to the expectation that different DOF's may be endowed with different levels of chaoticity above the SST, and with different levels of order below the SST. In the phase space, the region around the SST should be characterized by the coexistence of ordered and chaotic DOF's (these definitions are to be qualified by the time interval during which the system is observed, as asymptotically all DOF's should behave chaotically). The coexistence of ordered and chaotic dynamics in one and the same system was indeed detected already several years ago. For example, the dynamics of a lattice at low temperature exhibits such a mixed behavior if one describes it through the normal modes [10,11].

Summarizing this introduction, we can say that a thorough description of a dynamical system, both from mechanical and statistical points of view, requires the determination of the level of order or chaoticity of each single DOF. If the number of DOF's is low, one can use Poincaré's maps and auto-correlation and cross-correlation functions to characterize the dynamics of each DOF. But for systems with many DOF's these diagnostic tools become impracticable. On the other hand, the usual indicators of order and chaos (Lyapunov exponents, fractal dimension, and spectral entropy) are of global nature, and do not give information on single DOF's. One therefore has to resort to new diagnostic tools.

In a previous short paper [12], we introduced and computed *coherence angles* for Hamiltonian systems, which measure in the tangent space the angular distance between any physically relevant direction, and the direction of maximum divergence of trajectories starting from very near points. These angles can single out the DOF's that are characterized by the highest chaoticity, even above the SST. In the present paper we give a full account of the properties of the coherence angles, and show their connection with a set of *coherence times* characterizing each single DOF [13,14]. The main focus of the present work being the detailed analysis of the coexistence of ordered and chaotic DOF's, we have decided to apply this diagnostic tool to a system studied before, in order to interpret the results in the framework of a known phenomenology. In Sec. II we describe the Hamiltonian system chosen as a model for the present work; in Sec. III we study the transition region between highly chaotic and highly ordered dynamical regimes. Sections IV and V are devoted to coherence angles and their properties, and in Sec. VI we generalize this concept to a theoretical frame taking into account all Lyapunov characteristic directions—expanding and contracting—in the tangent space. Sec. VII is devoted to a discussion of the ''partial Lyapunov exponents'' (PLE's), which measure the rate of divergence of single DOF's; in the same section we show how to compute for each DOF a coherence time from the corresponding PLE, and its relation to the coherence angle. In Sec. VIII we summarize our method and the numerical results.

II. HAMILTONIAN MODEL

Atomic lattices are systems which are suitable for a detailed study of ordered and chaotic dynamics. Their behavior has been analyzed several years ago, and it has been found to exhibit a neat transition from a chaotic to an ordered regime when the energy is lowered [10,11]. For example it turned out that, in a 2D lattice, using a potential with parameters adapted to argon, the change in the dynamics takes place in a energy range corresponding to temperatures between 3 and 20 K [10,11]. A striking aspect of this transition was a breakdown at low temperature of the equipartition of energy among normal modes. The normal modes are (collective) variables which clearly manifest the change in the dynamical regime, and we have chosen them as an appropriate set to study the coexistence of order and chaos in a lattice with many degrees of freedom.

In order to allow comparison with previous work [10,11], we have first chosen for the simulation a 2D system composed of N^2 particles of mass M $(N=8)$, arranged on a square lattice with square cells of side d, surrounded by a border of fixed particles. Each particle is bonded to the four first neighbors by a Lennard-Jones (LJ) potential:

$$V(r)=4\varepsilon\left[\left(\frac{\sigma}{r}\right)^{12}-\left(\frac{\sigma}{r}\right)^{6}\right]; \tag{1}$$

$V(r)$ has its minimum at $r_0=2^{1/6}\sigma$.

Let us denote by u^x_{lm} and u^y_{lm} the displacements from the lattice equilibrium position of the particle at site (l,m) $(l,m=1,8)$. The normal-mode coordinates are defined by

$$q^x_{hk}=\frac{2}{N+1}\sum_{l,m=1}^{N} u^x_{lm}\sin\left(\frac{h\pi l}{N+1}\right)\sin\left(\frac{k\pi m}{N+1}\right),$$

$$q^y_{hk}=\frac{2}{N+1}\sum_{l,m=1}^{N} u^y_{lm}\sin\left(\frac{h\pi l}{N+1}\right)\sin\left(\frac{k\pi m}{N+1}\right),$$

where $h,k=1,N$. To obtain the expression of the Hamiltonian of the system in these coordinates, we expand the LJ potential to the second order around the first neighbors distance, and sum this contribution over all pairs of neighboring particles. The Hamiltonian now becomes

$$H=\frac{M}{2}\sum_{h,k=1}^{N}[(\dot{q}_{hk}^{x})^2+(\omega_{hk}^{x}q_{hk}^{x})^2+(\dot{q}_{hk}^{y})^2+(\omega_{hk}^{y}q_{hk}^{y})^2]+H',$$

where H' is the interaction Hamiltonian, which contains the whole coupling among modes produced by the interaction among particles (restricted to the first neighbors), and is negligible at low energy; $\omega_{hk}^{x},\omega_{hk}^{y}$ are the angular frequencies of the normal modes:

$$(\omega_{hk}^{x})^2=\frac{4}{M}\left[K_L\sin^2\frac{\pi h}{2(N+1)}+K_T\sin^2\frac{\pi k}{2(N+1)}\right],$$

$$(\omega_{hk}^{y})^2=\frac{4}{M}\left[K_L\sin^2\frac{\pi k}{2(N+1)}+K_T\sin^2\frac{\pi h}{2(N+1)}\right], \quad (2)$$

$$K_T\equiv\frac{1}{r}\frac{\partial V}{\partial r}\bigg|_d=48\left(0.5\frac{1}{d^8}-\frac{1}{d^{14}}\right),$$

$$K_L\equiv\frac{\partial^2 V}{\partial r^2}\bigg|_d=48\left(13\frac{1}{d^{14}}-3.5\frac{1}{d^8}\right).$$

We have considered two different cases for the cell side d.

(i) $d_1=r_0$, which corresponds to zero pressure at zero temperature. In this case $K_T=0$, and there are only N distinct frequencies ($\omega_{hk}^{x}=\omega_{kh}^{y}\equiv\omega_h$) ranging from 0.3789 to 2.1491 in LJ reduced units [15]; the normal modes are naturally divided into N groups, each including $2N=16$ modes of equal frequency. In terms of normal modes, the total energy of the system may be written as the sum of the energies E_h of each group of modes, plus the energy of the coupling due to the H' term; here

$$E_h=\sum_{k=1}^{N}[(\dot{q}_{hk}^{x})^2+(\omega_h^{x}q_{hk}^{x})^2+(\dot{q}_{kh}^{y})^2+(\omega_h^{y}q_{kh}^{y})^2].$$

In the following, the group energies E_h will be the variables used to monitor the chaos-to-order transition in the lattice. In fact, as described in Ref. [11], modes of equal frequency exchange rapidly their energy, providing a good energy equipartition inside a group; therefore, the energies of the groups become the relevant variables to evidence the breakdown of energy equipartition.

(ii) Compressing the system ($d<r_0$), one finds a critical value of the side cell d under which some frequencies become imaginary, i.e., the corresponding modes become unstable: this depends on the effect of both the changes in K_T and K_L. One has

$$K_T\geq 0 \text{ if } r\geq r_0,\quad K_T<0 \text{ if } r<r_0,$$

$$K_L\geq 0 \text{ if } r\leq r_f,\quad K_L<0 \text{ if } r>r_f,$$

where $r_f>r_0$ is the value corresponding to the inflection point of the LJ potential ($r_f=1.2445\sigma$). So in the case where $r<r_0$ or $r>r_f$ there exist some values of h and k such that $\omega_{hk}^2<0$. Restricting our attention to the case with $r<r_0$ (compressed lattice), we have estimated for the side cell a critical value corresponding to the onset of the instability. For the system with $N=8$ a Taylor expansion of K_T and of K_L to the first order in $d-r_0$ gives a critical value $d_2\simeq r_0-0.03r_0$ (see Appendix A for further details).

We have compressed the system to a value slightly above d_2. In this case the frequencies $\omega_{hk}^{x}=\omega_{kh}^{y}$ range from 0.0658 to 8.4471, and the relevant variables are the 64 group energies, where each group entails two modes of equal frequency:

$$E_{hk}=(\dot{q}_{hk}^{x})^2+(\omega_{hk}^{x}q_{hk}^{x})^2+(\dot{q}_{kh}^{y})^2+(\omega_{kh}^{y}q_{kh}^{y})^2.$$

We have used a standard central-difference algorithm for the numerical integration of the equations of motion of the particles, improved by one order in the computation of the velocities. A description of this modified algorithm is given in Appendix B.

We have explored the energy range from $e=0.2$ to 0.002, where $e=E/N^2$ is the energy per particle. This range includes the transition region determined in Refs. [10,11] for the 64-particle system. In this range we have studied the dynamics of the system at the energy values $e=0.2$, 0.05, 0.02, 0.007, and 0.002; for argon, this corresponds to temperatures in the range 0.24–24 K. In most simulations the total energy was initially distributed at random among all particles; as a consequence it was distributed at random among all normal modes. We have also performed some simulations in which only selected normal modes were initially excited (see Sec. III).

We have repeated our experiment for a 3D cubic lattice of 512 particles ($N=8$), with lattice parameter d_1; the normal modes' frequencies of this system are the same as in the 2D case, but the degeneration inside each group is 12 times higher ($3N^2=192$ modes per group); the temperature range explored has been the same as in the 2D case.

III. TRANSITION REGION

A. Generic initial conditions

In this section we analyze and complement previous work done on the transition region of our system, and show the interest of introducing new diagnostic tools suitable for gathering information on single DOF's. In Ref. [11] the authors analyzed the transition region of the system studied here, choosing generic intial conditions by distributing the energy at random among all the modes. They measured the energy of each group of modes, and computed all correlation functions:

$$G_{ij}(\tau)=\frac{\langle(E_i(t)-\langle E_i\rangle)(E_j(t+\tau)-\langle E_j\rangle)\rangle}{\sqrt{\langle(E_i(t)-\langle E_i\rangle)^2\rangle\langle(E_j(t+\tau)-\langle E_j\rangle)^2\rangle}};$$

here $\langle\cdot\rangle$ is a time average. The autocorrelation functions exhibit a twofold behavior: a rapid exponential-like decay at short times (which dominates at high energy), and a slow decay at long times (which dominates at low energy). The transition between the two regimes takes place in the temperature range mentioned in Sec. II. The threshold is different for different groups, and is generally higher for groups of higher frequency. The computation of the mean energy of each group of modes also allowed a check of the degree of equipartition reached by the system. Decreasing the tempera-

ture below 20 K, the system passes form a state where equipartition holds to states where equipartition requires increasing times; at low temperature no trend toward equipartition is visible. At the lowest energies studied the dynamics of the system is complex: at $e=2\times10^{-3}$, the behavior of the mean energies and of the cross-correlation functions highlights that nontrivial selection rules exist which greatly favor the energy exchange between some groups, and strongly hamper the other exchanges. These particular channels of energy exchange can be easily explained. In fact for $d=r_0$ there are exact resonances among the frequencies of the normal modes:

$$\omega_1+\omega_5=\omega_7,$$

$$\omega_2+\omega_4=\omega_8;$$

these resonances determine a preferred exchange among the resonant groups with respect to the others. Groups 3 and 6, which are not resonant, do not have an appreciable energy exchange, so that their energies are almost constant. Increasing the temperature the exchanges of energy become significant also outside the channels of resonance, and at about 20 K these channels disappear and equipartition is reached in a short time.

The diagnostic tools described so far—correlation functions and time dependence of mean energies—are useful if one deals with a system of few DOF's, but become impraticable if the number of DOF's becomes large. In order to have a synthetic description of the transition region, we have computed the spectral entropy, defined by

$$H(t)=-\sum_k p_k \ln p_k \quad \text{where } p_k=\frac{\langle E_k(t)\rangle}{\sum_k \langle E_k(t)\rangle}.$$

It is always positive, restricted between the value 0, when the energy is concentrated in only one group, and the value $H_{max}=\ln N$, when the system has reached equipartition and $p_k=(1/N)\ \forall k$. It gives a neat information about the degree of equipartition of the system, but it has an explicit dependence on N. To compare systems with a different number of distinct group frequencies, one introduces a normalized spectral entropy $\eta(t)$ for random initial conditions, where the explicit dependence on N is removed:

$$\tilde{\eta}(t)=\frac{H_{max}-H(t)}{H_{max}}.$$

At equipartition the time average of $\tilde{\eta}$ is equal to zero, while $\tilde{\eta}=1$ if all the energy is concentrated in only one group.

The results obtained for $\tilde{\eta}$ from the simulations of the 2D lattice, with random initial conditions, are shown in Fig. 1. As expected, the values of $\tilde{\eta}$ decrease as the temperature increases; $\tilde{\eta}$ first decreases almost exponentially, up to a temperature corresponding to about $e\simeq0.05$. Above this value, $\tilde{\eta}$ has a (slowly decreasing) value near to zero. This transition corresponds to the SST, which can be located between $e=2\times10^{-2}$ and 5×10^{-2} for this lattice.

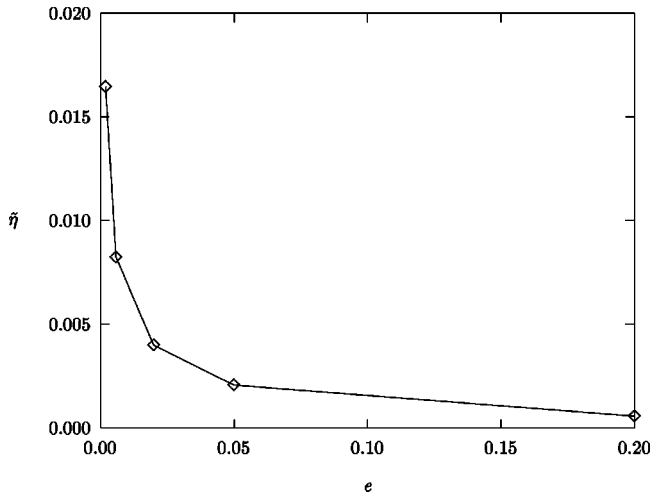

FIG. 1. Spectral entropy $\tilde{\eta}$ of an uncompressed 64-particles 2D system with random initial conditions, as a function of the energy per particle e.

We have simulated the cubic system with lattice parameter d_1 in three dimensions. In Fig. 2 we report the fraction of the total energy of all groups at $e=2\times10^{-2}$ for the 2D lattice and $e=3\times10^{-2}$ for the 3D lattice, both uncompressed. These specific energies correspond to $T=2.4$ K for both lattices, which exhibit at this temperature a slow trend toward equipartition. It is evident that, at any given time, the level of equipartition is higher for the 3D lattice than for the 2D one. We can try to understand this fact by considering that the exchanges of energy among groups of modes depend on the number of coupling terms among modes of different frequency. In an uncompressed 2D ($N\times N$) lattice there are $2N^2$ normal modes and N groups, each of $2N$ degenerate modes; the number of coupling terms (of the third order) between one mode and other modes of different frequency is $4N^3(N-1)$.

In a 3D ($N\times N\times N$) lattice there are $3N^3$ normal modes, and N groups of $3N^2$ degenerate modes each; the number of coupling terms between one mode and other modes of different frequency is $9N^5(N-1)$. The ratio of the numbers of coupling terms—involving different frequencies—in the 3D and 2D cases is therefore $9N^2/4$ ($=144$ for $N=8$). We can then infer that, for a given N and set of frequencies, in a 3D lattice the exchange of energy among different groups is more effective than in a the 2D lattice, because of the much higher number of coupling terms. As a matter of fact, this is what we found in the simulation by computing the spectral entropy. In the 3D lattice we obtained values of $\tilde{\eta}$ which are quite a bit lower than those of the 2D lattice. So, for example, we found $\tilde{\eta}=2.5\times10^{-4}$ at $e=0.02$, and $\tilde{\eta}=4.5\times10^{-5}$ at $e=0.03$. The latter value must be compared with $\tilde{\eta}=4.0\times10^{-3}$ found in the 2D lattice at $e=0.02$, which corresponds to the same temperature.

We have also computed the maximum Lyapunov exponent λ_1, which gives a measure of the rate of divergence in the phase space of initially nearby trajectories, and hence a measure of the degree of chaoticity of a dynamical system as a whole (λ_1 will be better defined in Sec. IV). A positive value of λ_1 means that trajectories starting from close points in $\Re^m$ will diverge exponentially in time, which is character-

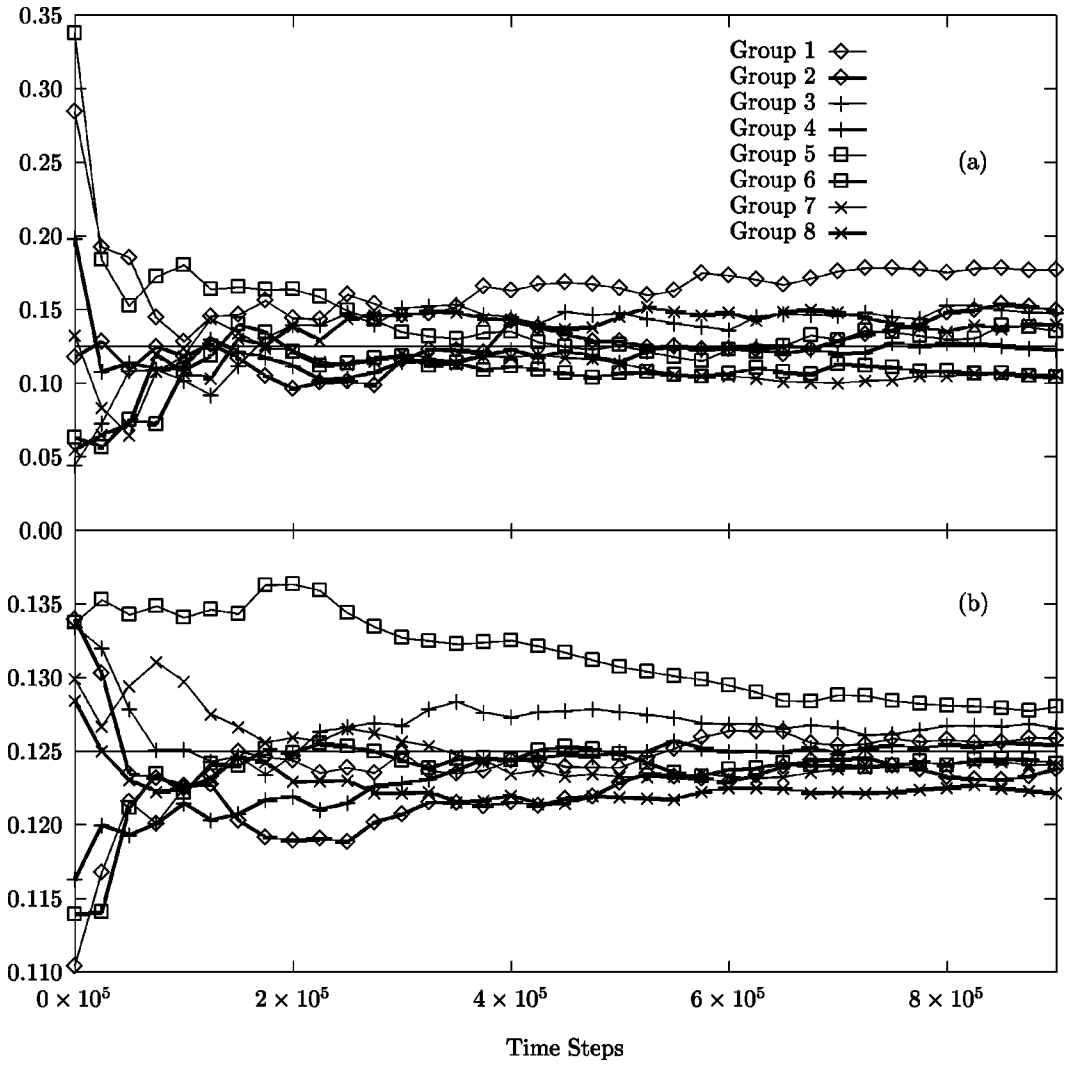

FIG. 2. Time averaged fraction of the total energy entailed in eight groups of modes: (a) 2D lattice with 64 particles and $e=0.02$; (b) 3D lattice with 512 particles and $e=0.03$. The horizontal line corresponds to 1/8 (equipartition).

istic of chaos. A zero value of λ_1 means that nearby trajectories diverge linearly in time, which is characteristic for order.

In Fig. 3 we report λ_1 vs the energy per DOF for the uncompressed 2D system (i.e., $d=d_1$), the compressed one ($d \geqslant d_2$), and the 3D uncompressed system. We observe the expected decrease with temperature of λ_1, and also a nonzero value at the lowest energy. This means that the system is still in a weakly chaotic regime, even though the behavior of $\{E_n\}$ shows that at this energy equipartition could be reached only in exceedingly long times.

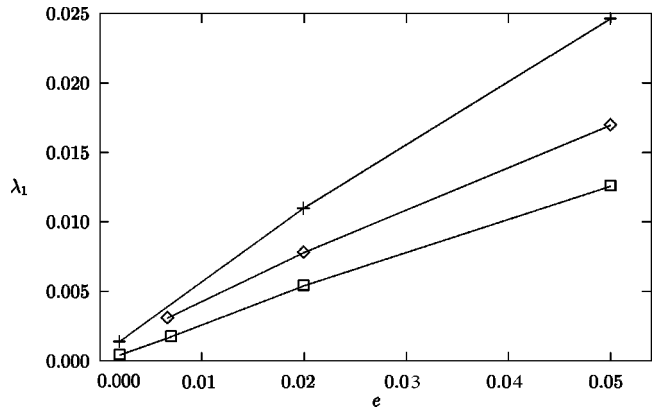

FIG. 3. Maximum Lyapunov exponent λ_1 as a function of the energy per degree of freedom, for the 2D uncompressed ($\square$) and compressed systems ($+$), and for the 3D system ($\diamond$).

The compressed system is more chaotic than the other two systems, as shown by the higher value of λ_1; this is probably due to an increase of the anharmonicity of the potential well ''felt'' by the particles, which more than compensates for a possible weaker exchange among modes due to the breakdown of the resonances among modes and among groups of modes. The behavior of λ_1 suggests locating the SST in the energy region where the slope of a curve λ_1 versus log$e$ changes: above the SST the slope of λ_1 will be lower, as the system is strongly chaotic and λ_1 changes less when the energy is raised [8]. Here the change of slope cannot be located exactly. One can only say that it takes place between $e=0.02$ and $e=0.05$, which agrees with the range indicated by the curve of the spectral entropy. The same figure shows the curve of λ_1 for the 3D system. Here the values of λ_1 are always higher than those of the 2D uncompressed system, as expected.

B. Nongeneric initial conditions

The previous measures allow a quantitative estimate of chaos and order for the system as a whole. But in a nonlinear system individual DOF's may behave differently, and interact with the other DOF's through a very complicated pattern of energy exchanges. This can be emphasized by setting the system in an initial state where only a few DOF's are excited, instead of using a generic condition in which the energy is randomly distributed among all DOF's. By doing this, the system is put in a phase space region of low probability density; nevertheless, this can yield interesting information, complementary to that gathered in the (generic) region of high probability density.

In Ref. [10] the transition region was analyzed, choosing initial conditions where all the energy E was given to modes belonging to one and the same group. During the dynamics the time averages $\langle E_h \rangle$ of the energy of each group of modes, defined in Sec. II, were monitored. It was found that inside each group of degenerate modes equipartition was reached quite fast, also at low temperature.

A parameter $\lambda = (E^{max} - E^{min})/E^{max}$ was used to measure the oscillation of the energy of the initially excited group of modes. E^{max} and E^{min} denote, respectively, the maximal and minimal energies attained by the initially excited group of modes during the evolution of the system. When $\lambda = 0$ this group does not share its energy with any other group, while when $\lambda = 1$ there is at least a time when this group has given all its energy to other groups.

A second parameter, $\mu = (\langle E_{n'} \rangle - \langle E_{n''} \rangle)/\langle E_{n'} \rangle$, measured the deviation from complete energy equipartition among modes. Here n' and n'' are the indices of the groups with, respectively, maximum and minimum time averaged energy $\langle E_n \rangle$. When $\mu = 1$ there is at least a group of modes which does not receive any energy during the whole simulation; $\mu = 0$ means that all groups share energy equally, i.e., that equipartition holds. Small values of λ imply large values of μ, but it can happen that both parameters are close to 1, when the initially excited group shares its energy with other groups but not with all of them.

In order to determine the boundary between ordered and stochastic motion as a function of the specific energy e, the behavior of λ and μ was observed fixing a threshold at $\lambda = \mu = \frac{1}{2}$. The results show that the thresholds grow with the frequency, except in the presence of resonances which create specific channels of energy exchange. The threshold energies found in this way locate the transition region in the same temperature range mentioned before.

Our simulation in two dimensions with cell side $d = d_1$ shows that preferred channels of energy exchange exist, which are dependent on the initially excited group; moreover, these channels are not symmetric. In Table I we report the results obtained at $e = 2 \times 10^{-3}$, which clearly show a striking strong asymmetry in the energy exchanges. If we initially excite only group 1, the energy flows to groups 2, 3, and 4, but group 1 does not receive any energy if we excite any other group. The resonant groups 2-4-8 exchange energy among themselves, but also with other groups. Group 3, one of the nonresonant groups, receives energy when we initially excite group 1, 5, or 8, but gives its energy only to group 6 when initially excited. Group 6, the other nonresonant one, takes energy if we excite groups 2, 3, or 4 but, when initially excited, does not exchange with any other group; this is an example of a phenomenon typical of nonlinear systems: the self-trapping of energy. It was already known that there is a lower threshold for the energy exchange among groups which depends on the initially excited groups: those with no initial energy unlikely absorb energy from other groups [10]. Table I emphasizes a sort of diffused self-trapping of energy, and adds the feature of a high asymmetry in those exchanges. Even when a group is excited whose frequency is in an exact resonance relation with other frequencies, its energy does not flow to all the resonant groups. Instead, it may flow to groups which are not resonant. So, for example, the first column of Table I shows that energy given initially only to group 1 goes to groups 2, 3, and 4 (which are not resonant), but not to groups 5 and 7 (which are resonant). This behavior is clearly due to the particular out-of-equilibrium initial conditions. For generic equilibriumlike initial conditions, group 1 would exchange energy mainly with the resonant groups 5 and 7, as shown in Ref. [11].

TABLE I. Exchanges of energy for different initially excited groups; the groups which receive energy are listed in order of decreasing average energy $\langle E_n \rangle$. $e = 0.002$.

	Initially excited group							
	1	2	3	4	5	6	7	8
Groups receiving energy	2	4	6	8	8		4	2
	3	6		6	3			3
	4							

The different response of the system to different nongeneric initial conditions can also be seen also in the behavior of the spectral entropy H and of λ_1. For initial conditions which are not random $[H_{max} \neq H(0)]$, one uses a different normalization of the spectral entropy:

$$\eta(t) = \frac{H_{max} - H(t)}{H_{max} - H(0)}.$$

In Fig. 4, $\eta(t)$ is shown at the energies 2×10^{-3} and 2×10^{-1}, for two different initial conditions. At $e = 2 \times 10^{-3}$, if only group 6 is initially excited, $\eta(t)$ is almost constant and equal to its maximum, due to the absence of any energy exchange; if group 1 is initially excited, η soon acquires a low value, due to the existence of a substantial energy exchange among groups. At higher energy, $e = 0.2$, the system tends to equipartition with both initial conditions, but it turns out that it needs very different times to relax to equilibrium. In the specific case, the relaxation time of η, when group 6 is initially excited, is one order of magnitude larger than the relaxation time found when group 1 is the only one initially excited.

Correspondingly, $\lambda_1(t)$ at $e = 0.002$ assumes a higher value (chaotic dynamics) for initial excitation of group 1, and a lower value (ordered dynamics) for initial excitation of group 6 (Fig. 5). Both results for η and λ_1 are in agreement with the characteristics of the two groups reported in Table I. At the energy $e = 0.2$, λ_1 soon reaches the same asymptotic value, when only group 1 or group 6 are initially excited. At this energy the dynamics of the system is chaotic,

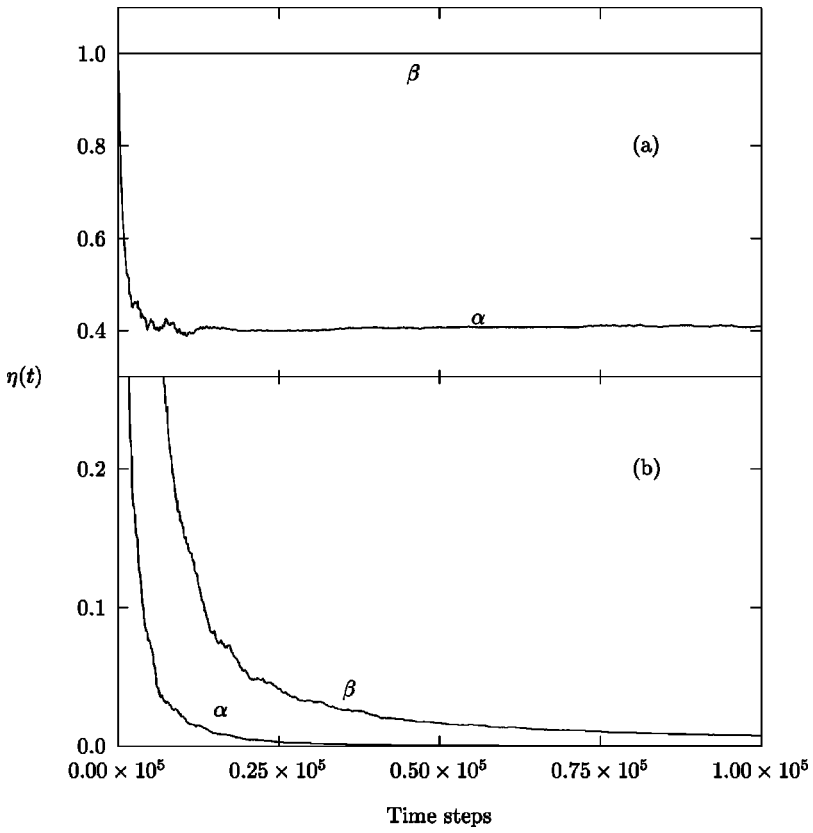

FIG. 4. Time evolution of the spectral entropy for a 2D lattice with out-of-equilibrium initial conditions: curves α and β correspond to simulations in which group 1 and, respectively; group 6 was the only one initially excited. (a) $e = 0.002$. (b) $e = 0.2$.

and the pattern of asymmetric channels which dominates the exchanges at low energy is destroyed.

As a conclusion to this section, we can say that the behavior of the lattice in the transition region is highly inhomogeneous, and that a detailed analysis of the transition region requires an examination of the single DOF's. The usual indicators of order and chaos, on the other hand, are of global nature, and give information only about the system as a whole. In Sec. IV we describe a tool suitable for characterizing single DOF's, which can also be used for systems with many DOF's.

IV. COHERENCE ANGLES

A. Dynamics in the tangent space

We first briefly recall the theory of the Lyapunov exponents, and elaborate on it to introduce the new diagnostic

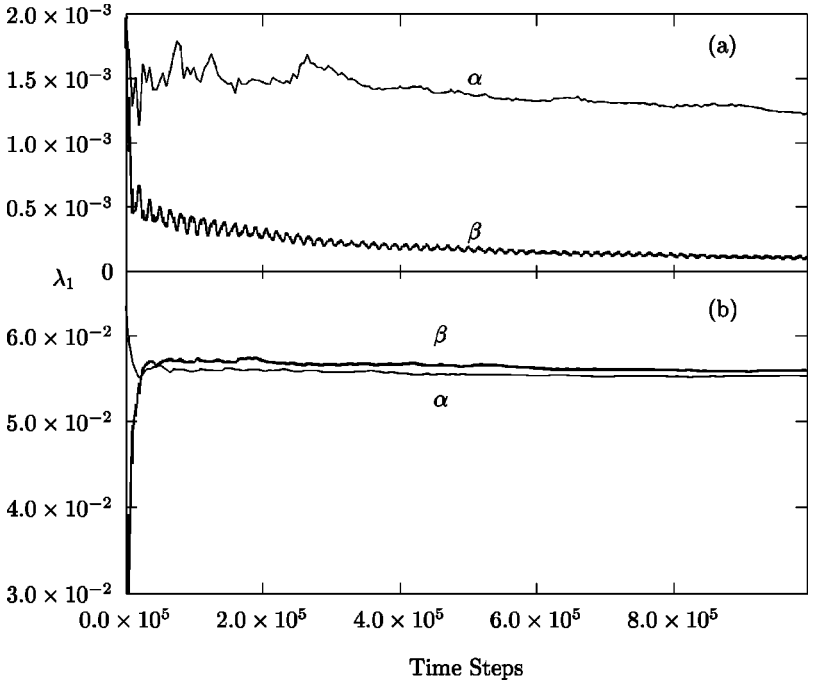

FIG. 5. Maximum Lyapunov exponent for nongeneric initial conditions; α: only group 1 is initially excited; β: only group 6 is initially excited. (a) $e = 0.002$. (b) $e = 0.2$.

tool. Let $\Re^m$ be a differentiable, m-dimensional, compact and connected Riemannian manifold of class C^2. If $\mathbf{x}\in\Re^m$, we denote by $T\Re^m_{\mathbf{x}}$ the normed tangent space to $\Re^m$ in $\mathbf{x}$. Let $\Phi^t:\Re^m\to\Re^m$ be a flow generated by the set of differential equations $\dot{\mathbf{x}}=\mathbf{f}(\mathbf{x})$; the tangent mapping of $T\Re^m_{\mathbf{x}}$ onto $T\Re^m_{\Phi^t_{\mathbf{x}}}$, induced by the diffeomorfism Φ^t, will be denoted by $d\Phi^t_x$.

Oseledec [16] (also see Ref. [17]) proved that a base $\mathbf{e}_\alpha$ exists in $T\Re^m_{\mathbf{x}}$, such that

$$\lim_{t\to\infty}\frac{1}{t}\ln\|d\Phi^t_x(\mathbf{e}_\alpha)\|=\lambda(\mathbf{x},\mathbf{e}_\alpha)=\lambda_\alpha(\mathbf{x}).$$

The numbers $\lambda_\alpha(\mathbf{x})$ are called the Lyapunov characteristic exponents, and give a measure of the rate of divergence in the phase space of initially nearby trajectories. $\lambda_\alpha(\mathbf{x})$ are not necessarily distinct; we denote by $\{\nu_j\}_{1\leqslant j\leqslant s}$ the distinct values taken by $\{\lambda_\alpha(\mathbf{x})\}_{1\leqslant\alpha\leqslant m}$, and by $k_j(\mathbf{x})$ the multiplicity of $\nu_j(x)$. We also let $\nu_i\geqslant\nu_j$ if $i\leqslant j$. Then a theorem [17] states that there exist linear subspaces $H_1,\ldots,H_s$, $s=s(\mathbf{x})$ such that $T\Re^m_{\mathbf{x}}=H_1\oplus\cdots\oplus H_s$ and dim $H_i=k_i(\mathbf{x})$. If $\mathbf{e}\neq 0$, $\mathbf{e}\in H_1\oplus H_2\oplus\cdots\oplus H_j$ but $\mathbf{e}\neq\in H_1\oplus H_2\oplus\cdots\oplus H_{j-1}$, then $\lambda(\mathbf{x},\mathbf{e})=\nu_j(\mathbf{x})$. If in $T\Re^m_{\mathbf{x}}$ one chooses a vector $\mathbf{e}$ at random, then one may expect to find $\lambda(\mathbf{x},\mathbf{e})=\lambda_1$. From now on $\{\nu_j\}$ will be denoted by $\{\lambda_j\}$.

The first way to compute the Lyapunov exponent was to follow the dynamics of two initially nearby trajectories, and to study the evolution of their distance. Later a second way was developed, in which the dynamics in the tangent space of the phase space was computed by linearizing the equations of motion. If $\dot{\mathbf{x}}=\mathbf{f}(\mathbf{x})$, $\mathbf{x}\in\Re^m$, the linear evolution of a tangent vector $\mathbf{w}\in T\Re^m_x$, the tangent space in $\mathbf{x}$, is given by

$$\dot{w}_i(t)=\sum_{j=1}^{m}\frac{\partial f_i}{\partial x_j}w_j(t).$$

From the theorems mentioned before, there is a base $\{\hat{\mathbf{e}}_i\}$ in $T\Re^m_{\mathbf{x}(0)}$, such that for almost all initial conditions the long time evolution of $\mathbf{w}$ is given by a superposition of vectors, the coefficients of which are exponentials of the Lyapunov exponents λ_ι,

$$\mathbf{w}(t)=\sum_{i=1}^{s}\mathbf{a}_i(t)e^{\lambda_i t}=\sum_{i=1}^{s}\mathbf{a}_i(t)e^{(\lambda_i-\lambda_1)t}e^{\lambda_1 t}\equiv\mathbf{b}(t)e^{\lambda_1 t},$$

where $s\leqslant m$, $\mathbf{a}_i\equiv\Sigma_j|\mathbf{w}(0)|c_j(t)\hat{\mathbf{e}}_j$, and this sum is done over all $\hat{\mathbf{e}}_j$ characterized by the same expansion rate λ_i. The matrices $\mathbf{c}_j(t)$ entail a possible time dependence weaker than the exponential one, and the rotation of $\{\hat{\mathbf{e}}_j\}$ generated by the flow of the dynamics. One has $\lim_{t\to\infty}\mathbf{b}(t)=\mathbf{a}_1(t)$ for almost all $\mathbf{w}(0)$.

Let the phase space be decomposed into the direct sum of n subspaces, S_1, S_2, ..., S_n ($n\leqslant m$), which are physically interesting for the study of the system (they can also be single DOF's). This phase space decomposition will induce an analogous decomposition of the tangent space in n subspaces TS_1, TS_2, ..., TS_n.

The *coherence angles* (CA's) α_i, $i=1,\ldots,n$, are defined through

$$\cos^2\alpha_i=\lim_{t\to\infty}\frac{1}{t}\int_0^t\frac{|\mathbf{w}^{(i)}(t')|^2}{|\mathbf{w}(t')|^2}dt',$$

where $\mathbf{w}^{(i)}(t)$ is the projection of $\mathbf{w}(t)$ on TS_i. Asymptotically $\mathbf{w}(t)\to\mathbf{a}_1(t)\exp(\lambda_1 t)$ and $\mathbf{w}^{(i)}(t)\to\mathbf{a}_1^{(i)}\exp(\lambda_1 t)$, where $\mathbf{a}_1^{(i)}$ is the projection of $\mathbf{a}_1$ on TS_i. So we have that

$$\cos^2\alpha_i=\lim_{t\to\infty}\frac{1}{t}\int_0^t\frac{|\mathbf{a}_1^{(i)}(t')|^2}{|\mathbf{a}_1(t')|^2}dt',$$

and each α_i represents an average angle between the subspace TS_i and the maximum expansion subspace. TS_i are a fixed characteristic of the system; the maximum expansion subspace depends only on the phase space representative point, and oscillates—as will be shown below—around an average direction in $T\Re^m_{\mathbf{x}(t)}$. It follows that the CA's have a weak dependence on the initial conditions in the tangent space and in the phase space.

The coherence angles provide a mean to single out those DOF's which are endowed with a higher degree of chaoticity, characterized by a low value of the angle. By contrast, DOF's characterized by a high value of the coherence angles have a high degree of coherence, and therefore require very long times to reach equilibrium. The latter DOF's are thus responsible for a possible finite-time out-of-equilibrium behavior of systems which are apparently at equilibrium—being chaotic as a whole, as indicated by a positive value of λ_1. There is, however, a problem in measuring accurately the degree of coherence of the most ordered DOF's, when the number n of physically interesting DOF's becomes very large. One can define a coherence angle α averaged on all the DOF's of the system, for which the relation $\cos\alpha=1/\sqrt{n}$ holds [12]. This implies that when n becomes large the most coherent DOF's are characterized by angles confined in a narrow range between α and $\pi/2$; they are thus difficult to distinguish, even if they are endowed with very different degrees of coherence (this does not apply to the most chaotic DOF's, which are characterized by low values of the α_i; therefore, their spread in the range $0-\alpha$ may increase when n increases). In the following we will show how to circumvent this problem.

B. Oscillation of the maximum expansion subspace

Let $A(t)$ be a function with zero time average

$$\lim_{t\to\infty}\frac{1}{t}\int_0^t A(t')dt'=0;$$

there are two distinct possibilities for lim $t\to\infty A(t)$: (i) either the limit is zero, or (ii) the function has no limit and oscillates indefinitely between positive and negative values. On the other hand, if (iii) $\lim_{t\to\infty}1/t\int_0^t|A(t')|dt'>0$, one can be sure that $A(t)$ has property (ii).

Let us consider the function

$$A_i(t_k)=\ln\frac{\cos\beta_i(t_k)}{\cos\beta_i(t_{k-1})}.$$

Here $\beta_i(t)$ is the angle at time t between a vector in the tangent space and its projection on the ith subspace TS_i: $\cos\beta_i(t)=|\mathbf{w}^{(i)}(t)|/|\mathbf{w}(t)|$.

We will now prove that

$$\lim_{t\to\infty}\frac{1}{t}\int_0^t A_i(t')dt'=0.$$

One has $\cos\beta_i(t_k)=\exp[A_i(t_k)]\cos\beta_i(t_{k-1})$ and

$$\cos\beta_i(t_T)=\exp\left[\sum_{k=1}^{T}A_i(t_k)\right]\cos\beta_i(t_0),$$

which is equivalent to

$$\frac{|\mathbf{w}_i(t_T)|}{|\mathbf{w}_i(t_0)|}=\exp\left[\sum_{k=1}^{T}A_i(t_k)\right]\frac{|\mathbf{w}(t_T)|}{|\mathbf{w}(t_0)|}.$$

Taking the logarithm and dividing by $t_T=T\triangle t$ ($\triangle t$ is the time step of the simulation), one has:

$$\frac{1}{t_T}\ln\frac{|\mathbf{w}_i(t_T)|}{|\mathbf{w}_i(t_0)|}=\frac{\sum_{k=1}^{T}A_i(t_k)}{T}\frac{1}{\triangle t}+\frac{1}{t_T}\ln\frac{|\mathbf{w}(t_T)|}{|\mathbf{w}(t_0)|}.$$

Asymptotically $T\gg 1$, so that

$$\lim_{t\to\infty}\frac{1}{t}\ln\frac{|\mathbf{w}_i(t)|}{|\mathbf{w}_i(t_0)|}=\langle A_i(t)\rangle_t\frac{1}{\triangle t}+\lim_{t\to\infty}\frac{1}{t}\ln\frac{|\mathbf{w}(t)|}{|\mathbf{w}(t_0)|}$$

and hence $\lambda_1=\langle A_i(t)\rangle_t(1/\triangle t)+\lambda_1$, from which it follows that $\langle A_i(t)\rangle_t=0$. From our numerical results (Sec. V D) we know that property (iii) holds. Therefore, property (ii) also holds. One can conclude that $A_i(t)$, $\forall\ i$ oscillates indefinitely around zero. This implies that $\cos\beta_i$ oscillates around its quadratic average value $\cos\alpha_i$, that is, that the angle between the vector $\mathbf{w}$ and the subspace TS_i oscillates around a mean value.

The tangent vector of the system $\mathbf{w}(t)$ follows the maximum expansion subspace H_1, which oscillates around its average orientation. This point can be checked in the following way. There are no prescriptions in the Lyapunov theory about the norm one chooses in the tangent space, provided there exists one. Hence we can choose a norm such that

$$|\mathbf{w}(t)|^2=\sum_{i,j}(\delta\dot{q}_{ij}^2+\omega_{ij}^2\delta q_{ij}^2),$$

where δq_{ij} are the normal coordinates in the tangent space, and ω_{ij} the corresponding frequencies. With this choice of the norm we expect to minimize the oscillation characteristic of the normal mode, leaving only the variation due to expansion in the tangent space. At low energy, where the normal modes approximation is good, we find that the asymptotic dependence of $|\mathbf{w}(t)|$ on time is of the form $e^{\lambda_1 t}$. This means that $\mathbf{w}(t)$ belongs to H_1; therefore, the oscillations of $\beta_i(t)$ can only be due to the oscillation of the maximum expansion subspace H_1 around its average orientation.

V. NUMERICAL RESULTS FOR THE COHERENCE ANGLES

In this section we describe the results of the CA's relative to groups of normal modes; they have been obtained from numerical simulations at various energies for 2D and 3D lattices, with lattice parameters d_1 and d_2 (uncompressed and compressed lattice). Different initial conditions were used at a given energy both in the phase space and in the tangent space. We have computed the dynamics of one trajectory for each initial condition in the phase space, and used the tangent dynamics (assuming that the second one starts at an infinitely small distance). For the systems we deal with, the equations of motion in the tangent space are reported in Appendix C.

A. CA's for the uncompressed 2D lattice

CA's have been computed for different random initial conditions, either in the tangent or in the phase space, at every simulated energy (Sec. II). In Fig. 1 of Ref. [12] the spectrum of the CA's at three different energies was reported. The CA's show, as expected, a very weak dependence on the initial condition in the tangent space: lowering the energy, the maximum relative spread of their values increases from 10^{-6} at $e=0.2$ to 0.04 at $e=0.002$. The dependence on the initial point in the phase space (at a given energy) is stronger: the maximum relative spread increases from 0.005 at $e=0.2$ to 0.08 at $e=0.002$.

The spectrum below the SST ($e=0.002$) exhibits a variegated structure where group 1 has the lowest CA and hence is the most chaotic, followed by group 2, which has the second lowest CA. On the other hand groups 3 and 6, which have the highest CA's, should be the most ordered; this result is confirmed by the behavior of the same groups found in previous work [11]: their energies are almost constant. A spectrum taken at $e=0.007$ shows that group 3 has lost its ordered behavior, and is now the third most chaotic group after groups 1 and 2, while group 6 is still quite ordered. Near the SST ($e=0.02,0.05$) one observes a monotonous increase of coherence with the frequency of the normal modes: group 3 and 6 have lost their singular behavior. Raising the energy above the SST ($e=0.2$), we observe that all normal modes have similar coherence, with the exception of group 1, which still is more chaotic.

Besides the CA's of the groups, we also computed the CA's for the 64 pairs of x and y modes characterized by the same frequency and by the same wave vector [same indices h and k for ω_{hk}^x and ω_{kh}^y in formula (2)], and the results are shown in Fig. 6. They agree qualitatively with those found for the groups, but the spread of the values is reduced; the average angle is of course higher, because of the higher number of DOF's ($\cos\alpha=1/\sqrt{64}$, $\alpha\simeq 83°$). At the lowest energy ($e=0.002$), modes 1–8, which constitute group 1 in this lattice, are definitely the most chaotic. On the other hand the CA's of modes 41–48 are the highest of the system and nearly equal, in agreement with the fact that group 6 is the most coherent and does not exchange energy with other modes outside the group, as its frequency is not resonant. The CA's of modes 17–24 (group 3, the other nonresonant one) also fall in a narrow range. Raising the energy to $e=0.02$ the CA's gradually increase with increasing values of

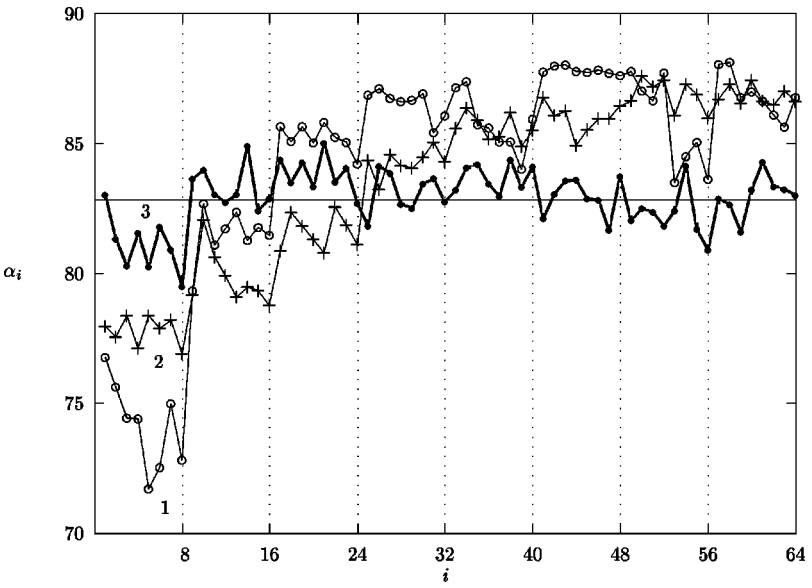

FIG. 6. Spectrum of the coherence angles for the uncompressed 2D lattice at energies: $e=0.002$ (1), $e=0.02$ (2), and $e=0.2$ (3). i is the index of pairs of modes characterized by the same frequency and by the same wave vector. The frequency increases with i, every eight pairs. The horizontal line corresponds to the average angle $\alpha \simeq 83°$.

frequency, even though inside each group there are small deviations from the expected trend [18,19]. At $e=0.2$ the equipartition is nearly reached and we find that all CA's are close to the average α.

B. CA's for the compressed 2D lattice

Compressing the system we destroy the exact resonances among frequencies, as mentioned in Sec. III A. In this case we have 64 groups of different frequency, each of two modes (x and y) of equal frequency and equal wave vector; the spectrum of the CA's gives at the same time a detailed characterization of all DOF's, and a synoptic view of the dynamical behavior of the whole system.

In Ref. [12] we reported the spectra of the CA's at two different energies: $e=0.002$ and 0.05. For this lattice the average angle is $\alpha \simeq 83°$. At the lowest energy pairs 1–8, which originate from group 1 of the uncompressed lattice, exhibit the lowest CA's; the highest frequency pairs are the most coherent, as expected. But we found an unexpected high chaoticity of two medium and high frequency bunches of pairs centered around pair Nos. 40 and 56. The higher chaoticity of pair Nos. 40 and 56 may be related to the fact that their frequencies are resonant (within 0.4%) with the ratio 3/2, which may lead to a strong exchange of energy. At the higher energy pairs 1–8 still exhibit CA's significantly lower than the rest of the system, where the CA's are very near to the average one. The coherence angles show here that even in this highly chaotic regime the different DOF's are characterized by different coherence levels. The spread of the CA's around the average angle in this system is lower than in the uncompressed one. According to the results found for the Lyapunov exponent (Sec. III), we can attribute this fact to a higher level of chaoticity of the compressed lattice with respect to the uncompressed one.

C. CA's for the 3D lattice

We have also computed CA's for an uncompressed 3D system of $N^3=512$ particles. The numerical results show that for a given frequency (i.e., for a given group of normal modes) the values of the CA's are almost the same as in the uncompressed 2D case. We remind the reader that we observed (see Sec. III) a higher degree of chaoticity of the 3D lattice with respect to the 2D one. Indeed the result $\lambda_1^{3D} > \lambda_1^{2D}$ means that a vector belonging to the maximum expansion subspace expands with a higher rate in the 3D system than in the 2D system; this is not related to the CA's, which are the angles between the maximum expansion subspace and the DOF subspaces, and measure the contribution of each DOF to the chaoticity of the whole system.

The CA's are computed through the ratio $|\mathbf{w}_i(t)|/|\mathbf{w}(t)|$. To understand why the CA's are nearly equal in two and three dimensions, one can suppose that the pace of evolution of $\mathbf{w}_i(t)$ depends, besides their frequency, on the number g_i of anharmonic terms in the Hamiltonian which involve modes of group i, while the pace of evolution of $\mathbf{w}(t)$ depends on the number g of all anharmonic terms of the system. For the purpose of comparison, the numbers g_i and g can be computed by considering only the third order terms in the expression of the Hamiltonian in normal modes, which give the highest contribution to the time evolution of the tangent vectors.

For the 2D lattice each group entails $2N$ modes, and $g_i = 8N^4(N-1)+(2N)^3$, where the first term is the number of third order terms involving modes of the group and modes of any other groups, while the second term is the number of third order terms inside the group. For the whole system one has $g=(2N^2)^3$. For the 3D lattice each group entails $3N^2$ modes, and $g_i=27N^7(N-1)+(3N^2)^3$; one also has $g=(3N^3)^3$. The ratio g_i/g in both cases is $[N(N-1)+1]/N^3=0.111$. The fact that the two values are equal is a hint that the CA's may depend on the fraction of anharmonic terms involving modes belonging to the corresponding subspace S, besides the known dependence on the frequency.

In the case of the compressed 2D lattice, the CA's are quite different from the uncompressed case, as one can see comparing Fig. 6 with Fig. 3 of Ref. [12]. As a matter of fact, one finds $g_i/g=0.0154$ for the compressed lattice, and also for the uncompressed one, when the latter is described by means of groups entailing only a pair of modes, as in

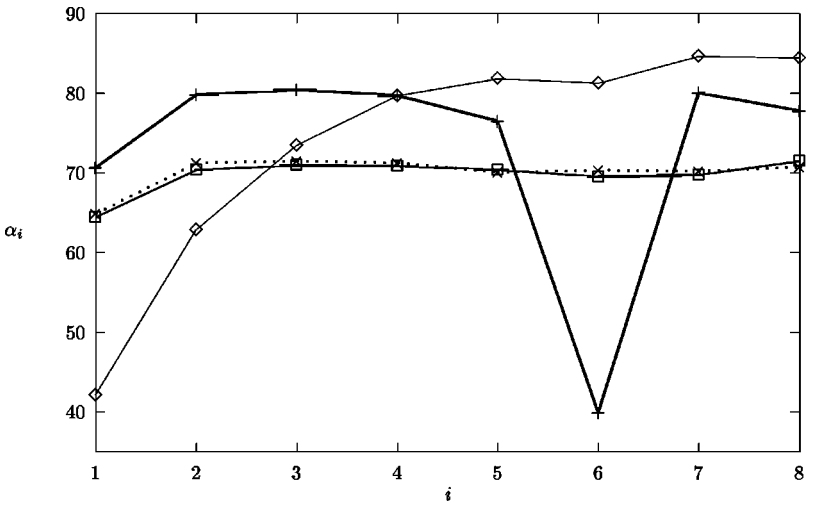

FIG. 7. Spectrum of the coherence angles for the uncompressed 2D lattice for nongeneric initial conditions. $e=0.002$; group 1 (6) initially excited: $\diamond$ (+). $e=0.2$; group 1 (6) initially excited: $\square$ ($\times$). i is the index of groups of modes characterized by the same frequency. The frequency increases with i.

Fig. 6. In this case, the difference between the CA's of the two systems is clearly only due to the different frequency spectra.

D. Oscillation of the maximum expansion subspace

The results obtained for the function $A_i(t)$ introduced in Sec. IV B show that the averages $\langle|A_i(t)|\rangle\ \forall\ i$ are well stabilized in the course of the simulations, and that they are always positive at all the energies studied; furthermore, the $\langle|A_i(t)|\rangle$ are different for different i. We can conclude that the maximum expansion subspace of each DOF oscillates in the tangent space of the hypersurface of constant energy. The amplitude of this oscillation is different depending on the subspace TS_i on which we project the tangent vector $\mathbf{w}(t)$. Raising the energy, the differences among amplitudes corresponding to different subspaces increase and decrease in an irregular way, while their average increases.

E. Nongeneric initial conditions

In this last subsection we briefly report the results obtained by exciting only one group at a time, in the uncompressed 2D lattice. In Fig. 7 the CA's at the energies $e=0.002$ and 0.2 are reported for initial excitation of group 1 or group 6. At the lowest energy group 1, if initially excited, is the most chaotic and from Table I we know that it gives its energy mainly to groups 2, 3, and 4 (the intensity of the exchange decreases in this order). The CA's are indeed found to be increasing in that same order. If we excite group 6, according to Table I the exchanges with other groups are very weak, and hence the CA's are very high. Obviously the lowest angle in this case is just that of the sixth group, which turns out to be even lower than that of group 1, when the latter is the only group initially excited. At the higher energy the two different initial conditions give nearly the same results. We note that the resulting CA's are quite similar to those obtained for random initial conditions (as shown in Fig. 1 of Ref. [12]): when equipartition holds the system is in a state which is no more sensitive to the initial conditions. The results of this subsection show that the CA's can provide a detailed information on the behavior of the system also when the latter is in a nonequilibrium dynamical state.

VI. GENERALIZED COHERENCE ANGLES

The CA's measure the angular distance between the various DOF's and the maximum expansion subspace H_1 corresponding to λ_1, and are well defined asymptotically. But in the medium time, the evolution of a tangent vector and of its projections on the DOF subspaces depends on its position relative to all the subspaces H_j, corresponding to the whole set of Lyapunov exponents. In condensed matter systems the Lyapunov spectrum is smooth: the exponents following the first have values slowly decreasing from the maximum one [20]. As the chaoticity of a DOF increases with its angular proximity in the tangent space to a rapidly expanding subspace, it is clear that one should also consider the subspaces H_j corresponding to expansion coefficients just below λ_1. More generally, one can expect the medium time behavior of a DOF to depend on its angular distance from all s subspaces H_j corresponding to Lyapunov exponents, whether expanding or contracting.

In Ref. [14] it has been shown how the coherence characterizing the lth DOF is the result of this medium time behavior, i.e., the behavior of $\mathbf{w}^{(l)}(t)$ before $\mathbf{w}(t)$ is definitely oriented along the $\hat{\mathbf{e}}_1$ direction, and hence the expansion rate of $\mathbf{w}^{(l)}(t)$ also has reached the value λ_1. In order to determine the behavior of $\mathbf{w}^{(l)}(t)$, one should compute the angles between each DOF and each subspace characterized by a Lyapunov exponent, but this is not easily practicable as one should exactly know the dynamics of these subspaces.

Alternatively, one can use an orthogonal set of vectors $\{\mathbf{v}_k\}$ $k=1,\ldots,m$, which expand with the Lyapunov exponents $\{\lambda_k\}$ (see Appendix D for more details). Let $\{\mathbf{v}_k\}$, $k=1,\ldots,m$, be an orthogonal set of vectors of the tangent space $T\mathfrak{R}^m_{\mathbf{x}}$ such that each $\mathbf{v}_k(t)$ expands (or contracts) asymptotically with the Lyapunov exponent λ_k: $\mathbf{v}_k(t)=u_k(t)\mathbf{v}_k(0)e^{\lambda_k t}$, where $u_k(t)$ is a unitary matrix describing the (possible) rotation of $\mathbf{v}_k$. The generic vector $\mathbf{w}$ of the tangent space can be initially decomposed in a sum of vectors lying along the vectors $\mathbf{v}_k$,

$$\mathbf{w}(0)=\sum_{k=1}^{m}\ [\mathbf{w}(0)\cdot\hat{\mathbf{v}}_k]\hat{\mathbf{v}}_k\equiv\sum_{k=1}^{m}\ w_k(0)\hat{\mathbf{v}}_k\,,$$

where $\hat{\mathbf{v}}_k \equiv \mathbf{v}_k / |\mathbf{v}_k(0)|$. As the equations of motion in the tangent space are linear, its asymptotic time evolution can be written as

$$\mathbf{w}(t) = \sum_{k=1}^{m} w_k(0)\hat{\mathbf{v}}_k(t) = \sum_{k=1}^{m} w_k(0)u_k(t)\hat{\mathbf{v}}_k(0)e^{\lambda_k t},$$

$$\frac{|\mathbf{w}(t)|}{|\mathbf{w}(0)|} = \left[\frac{\sum_{k=1}^{m} w_k^2(0)e^{2\lambda_k t}}{\sum_{k=1}^{m} w_k^2(0)} \right]^{1/2} \equiv e^{\lambda_e t}.$$

In this way for the vector $\mathbf{w}$ one defines an effective expansion coefficient λ_e, which depends on time and on the initial conditions:

$$\lambda_e(t) \equiv \frac{1}{2t} \ln \left[\frac{\sum_{k=1}^{m} w_k^2(0)e^{2\lambda_k t}}{\sum_{k=1}^{m} w_k^2(0)} \right].$$

Unless the initial direction of $\mathbf{w}(0)$ lies along a specific vector $\mathbf{v}_l$ of the base $[\mathbf{w}_k(0) = \delta_{kl}\mathbf{w}(0)]$, its evolution will be influenced by all Lyapunov exponents, and eventually only by λ_1.

One can now use for the vectors $\hat{\mathbf{v}}_k$ a decomposition on the orthonormal set $\hat{\mathbf{w}}^{(l)}$ of the DOF's: $\hat{\mathbf{v}}_k(t) = \Sigma_{l=1}^{n} \hat{\mathbf{w}}^{(l)} \cos \alpha_{kl}(t) e^{\lambda_k t}$, where α_{kl} is the angle between vector $\hat{\mathbf{v}}_k$ and the subspace TS_l, corresponding to the lth DOF or set of DOF's. Using the previous decomposition of $\mathbf{w}$, one finds

$$\mathbf{w}(t) = \sum_{k=1}^{m} w_k(0)\hat{\mathbf{v}}_k(t) = \sum_{l=1}^{n} \sum_{k=1}^{m} w_k(0) \cos \alpha_{kl}(t) e^{\lambda_k t} \hat{\mathbf{w}}^{(l)}$$
$$\equiv \sum_{l=1}^{n} w^{(l)}(t)\hat{\mathbf{w}}^{(l)},$$

where $w^{(l)}$ is the projection of $\mathbf{w}$ on TS_l. The asymptotic time evolution of the component of $\mathbf{w}(t)$ on the lth subspace can thus be represented through

$$\frac{|\mathbf{w}^{(l)}(t)|}{|\mathbf{w}^{(l)}(0)|} \equiv e^{\lambda_e^{(l)}(t)t}. \tag{3}$$

This defines $\lambda_e^{(l)}(t)$ as an effective expansion coefficient for the lth subspace of DOF's, which depends on time and on the initial condition:

$$\lambda_e^{(l)}(t) = \frac{1}{2t} \ln \left[\frac{\sum_{k=1}^{m} w_k^2(0) \cos^2 \alpha_{kl}(t) e^{2\lambda_k t}}{\sum_{k=1}^{m} w_k^2(0) \cos^2 \alpha_{kl}(0)} \right].$$

The complete set of angles $\{\alpha_{kl}\}$ characterizes completely the time evolution of all subspaces of the tangent space, but the computation of $n \times m$ terms can become a heavy task for large systems. In addition to the computational burden, using the whole set $\{\alpha_{kl}\}$ would make it impossible to take advantage of the synoptic view provided by a single coherence spectrum, the one entailing only the angles with the most expanding subspace [12]. Fortunately, the tangent space seems to be structurated in such a way that the angles between a generic tangent vector and the most expanding directions have similar values, and the same holds for the most contracting ones. By this we mean that the projection of a tangent vector on a subspace characterized by a given Lyapunov exponent turns out to be very similar in magnitude to the projection on another subspace characterized by a Lyapunov exponent similar to the previous one [21].

Moreover, the values of the projections on the most expanding vectors are grouped together, well distinct from values of the projections on the most contracting ones. If one assumes this to be a generic property of condensed matter systems, the CA's defined in Ref. [12] should also be indicative of the angles the DOF's make with the subspaces labeled by the Lyapunov exponents closely following the first (maximum) one; they should thus entail the relevant information on the degree of chaoticity, due to the angular distance from the most expanding directions.

VII. COHERENCE TIMES

In Sec. IV A we observed that when the number of DOF's n becomes very large, the average CA α increases toward $\pi/2$ (because $\cos\alpha = 1/\sqrt{n}$), and it is difficult to distinguish between the most ordered DOF's, even if they are characterized by very different degrees of coherence. Moreover, as α depends on n, it would be difficult to compare coherence properties of systems with different numbers of DOF's. Hence we have looked for a new tool independent of n, physically meaningful and entailing relevant information on the medium time behavior of the DOF's.

The natural starting point is given by the effective expansion coefficients $\lambda_e^{(l)}(t)$; as shown in Sec. VI, they synthesize—for each DOF—the effect of all expanding and contracting directions of the phase space. As shown by formula (3), $\lambda_e^{(l)}(t)$ characterizes the rate of divergence of the lth DOF for nearby trajectories, in the same way as $\lambda_e(t)$ does for the total divergence of the trajectories.

In analogy with the Lyapunov exponents, one defines PLE's for single DOFs [13]:

$$\lambda^{(l)} \equiv \lim_{t\to\infty} \lambda_e^{(l)}(t) = \lim_{t\to\infty} \frac{1}{t} \ln \frac{|\mathbf{w}^{(l)}(t)|}{|\mathbf{w}^{(l)}(0)|}.$$

(From now on we drop the subscript e in the effective expansion coefficients λ) From the theorems quoted in Sec.

IV A, we can conclude that $\lambda^{(l)}=\lambda_1\ \forall\ l$ even if $\lambda^{(l)}(t)$ may differ substantially from λ_1. This difference, and the time needed to reach the regime where $\lambda^{(l)}\simeq\lambda_1$, characterize each DOF. The value $\lambda^{(l)}(t)$ gives information about the instantaneous exponential rate of expansion, which may be—before the relaxation—lower or higher than that of the whole system. Hence we could have characterized each DOF by the inverse of the average value of $\lambda^{(l)}(t)$, like λ_1^{-1} characterizes the total system. As the medium time expansion of $\mathbf{w}^{(l)}(t)$ is not an exponential, $\lambda^{(l)}(t)$ alone is not a good characterization of the lth DOF. On the other hand, $\lambda^{(l)}(t)\rightarrow\lambda_1$ almost anywhere in the tangent space, but the time t^* after which $\lambda^{(l)}(t)\simeq\lambda_1$, that is the time the DOF needs to reach the asymptotic expansion rate of the whole system, is difficult to determine, as there is not a neat transition to the asymptotic behavior [14]. A way to characterize a DOF taking into account both these quantities could be to compute the area of the region between $\lambda^{(l)}(t)$ and $\lambda(t)$. We made an attempt to compute various quantities related to this area. Unfortunately it turned out that all these quantities were strongly dependent on the initial conditions, making any characterization of a pattern among DOF's impossible, even when we knew from previous results that there was one. Moreover, in order to compute this area, one would have to integrate in time from 0 to ∞, which means that one has to introduce a cutoff. In order to be meaningful, the result of the computation should have a good stability when the cutoff is varied in the region following the relaxation. On the contrary, we found quite often that the integral was not convergent and had a strong dependence on the cutoff.

Nevertheless, by observing the behavior of $\lambda^{(l)}(t)$ vs t, one can understand the approach to relaxation of each DOF. In Figs. 1 and 2 of Ref. [14] we gave the results obtained for some groups of DOF's at $e=0.2$ and 0.002. We reported

$$\ln\frac{|\mathbf{w}^{(l)}(t)|}{|\mathbf{w}^{(l)}(0)|}=t\lambda^{(l)}(t)$$

vs t, so that the slope of the curves gave $\lambda^{(l)}(t)$; the curves had been smoothed by coarse-graining values on a moving interval ranging over several periods of the normal modes. At the highest energy, where the whole system is in the chaotic regime, all subspaces behave alike, and the curves corresponding to $\lambda^{(l)}(t)$ are fairly similar to the global one relative to $\lambda(t)$, an almost straight line with slope λ_1; still, a small but definite difference among DOF's is evident. At the lowest energy this difference is more visible, and one can observe a differentiated behavior of the DOF's, typical for a partially ordered dynamics.

In the case where the distinction among the DOF's is well defined, one can suppose that for each group a time t_l^* exists up to which $\lambda^{(l)}(t)$ evolves to λ_1, while $\lambda^{(l)}(t)=\lambda_1$ when $t>t_l^*$. The real situation is far from being so regular: the time t_l^* is not easily identificable, and one cannot define an average slope in the interval $0-t^*$. On the other hand, the distance between the lines $t\lambda^{(l)}(t)$ and $t\lambda(t)$ oscillates around its average value when $t\rightarrow\infty$. This distance is the result of the combined effect of the difference between each $\lambda^{(l)}(t)$ and $\lambda(t)$, and of the time t_l^* needed to relax; it is easily computable, and the precision of this measure increases with increasing averaging times [14].

TABLE II. Coherence times $\tilde{\tau}_l$ of the groups of normal modes, at specific energy e, for the 2D uncompressed lattice.

e	0.002	0.006	0.02	0.2
$\tilde{\tau}_1$	−355	−130	−29	12
$\tilde{\tau}_2$	808	346	135	26
$\tilde{\tau}_3$	2982	787	222	25
$\tilde{\tau}_4$	3186	1109	338	25
$\tilde{\tau}_5$	3079	1100	428	27
$\tilde{\tau}_6$	4776	1405	512	27
$\tilde{\tau}_7$	2878	1168	493	25
$\tilde{\tau}_8$	3333	1383	534	29
λ_1^{-1}	1563	560	231	24

A hierarchy of coherence among the DOF's can be established by computing, during the dynamics, the vertical distances between each line $\lambda^{(l)}t$ and the line $\lambda_1 t$, and averaging on time. The horizontal distances, which we call *time shifts*, are then obtained dividing the vertical distances by the average common slope λ_1:

$$\begin{aligned}\tau_l&=\frac{1}{\lambda_1}\lim_{t\rightarrow\infty}\frac{1}{t}\int_0^t\left(\ln\frac{|\mathbf{w}(t')|}{|\mathbf{w}(0)|}-\ln\frac{|\mathbf{w}^{(l)}(t')|}{|\mathbf{w}^{(l)}(0)|}\right)dt'\\&=\frac{1}{\lambda_1}\lim_{t\rightarrow\infty}\frac{1}{t}\int_0^t\left(\ln\frac{|\mathbf{w}(t')|}{|\mathbf{w}^{(l)}(t')|}-\ln\frac{|\mathbf{w}(0)|}{|\mathbf{w}^{(l)}(0)|}\right)dt'\\&=-\frac{1}{\lambda_1}\left(\left\langle\ln\frac{|\mathbf{w}^{(l)}(t')|}{|\mathbf{w}(t')|}\right\rangle_t-\ln\frac{|\mathbf{w}^{(l)}(0)|}{|\mathbf{w}(0)|}\right)\\&=-\frac{1}{\lambda_1}(\langle\ln|\cos\beta^{(l)}(t')|\rangle_t-\ln|\cos\beta^{(l)}(0)|).\end{aligned}\tag{4}$$

Here $\beta^{(l)}$ is the angle between the lth subspace and the generic vector $\mathbf{w}$. The first term in Eq. (4) has good convergence properties, like the coherence angles; but the second term in Eq. (4) depends strongly on the initial conditions in the tangent space, and may be large. One can get rid of the dependence on the initial conditions by averaging $\{\tau_l\}$ over many different $\mathbf{w}(0)$. We have computed τ_l of all subspaces at various specific energies; each value is an average over 15 initial conditions in the tangent space. For large enough times, the expansion rate of the distance for initially close trajectories is λ_1; a negative (positive) time shift means that the corresponding DOF's difference between initially close trajectories reaches a fixed level of expansion a time τ_l before (after) the whole system, i.e., the DOF is more chaotic (coherent) than the whole system.

τ_l can also be written

$$\tau_l=\frac{1}{\lambda_1}\lim_{t\rightarrow\infty}\frac{1}{t}\int_0^t t'[\lambda(t')-\lambda^{(l)}(t')]dt',$$

and coincide with the ''coherence times'' defined in a previous work [13]. However, from the numerical point of view, the two formulas are not equivalent, as the latter way of computing enhances numerical errors at short and long times. At short times the time-dependent Lyapunov exponents are numerically ill defined; at long times the difference between all partial Lyapunov exponents and the total one goes to zero, and is multiplied by a diverging time. These effects are so large that an interpretation of the results becomes difficult; on the other hand, computing the integrand through formula (4) gives well defined results at all energies studied.

In order to make a comparison among DOF's belonging to different states of a system, or to different systems, one also has to include the typical scale of chaoticity of each whole system, i.e. λ_1^{-1}; therefore, we define a *coherence time* as $\tilde{\tau}_l=(\lambda_1)^{-1}+\tau_l$. In Table II we report the $\tilde{\tau}_l$ of the groups of normal modes at four different energies. Some coherence times $\tilde{\tau}_l$ turn out to be negative, which is due to a negative time shift τ_l whose absolute value is larger than the average expansion rate λ_1^{-1}. This means that the corresponding group of normal modes reaches a given level of chaoticity in advance of $|\tau_l|$ with respect to the system considered as a whole, of course this is only meaningful for times larger than $|\tau_l|$. The coherence times increase, as expected, when the energy is lowered and the dynamics becomes more ordered. If one excludes the value at the highest energy ($e=0.2$), the other points show a dependence on the specific energy e which can roughly represented by a law $\tilde{\tau}_l \sim e^{-z_l}$, with $0.8<z_l<1.1$, depending on the group of normal modes. The coherence time of a DOF gives the order of magnitude of the time that this DOF needs to relax to equilibrium, in analogy with the time $(\lambda_1)^{-1}$ characterizing the relaxation of the whole system. The results shown in Table II, which entail the whole dynamics in the tangent space, are in agreement with those obtained by computing the CA's: group 1 is always the most chaotic; on the other hand, at high energy group 8 is the most choerent one, while at low energy it is group 6, as expected [12]. These results seem thus to confirm that the hierarchy among DOF's obtained by considering only the maximum expansion subspace, i.e., that given by the CA's, is representative of all the most expanding directions, as advanced in Sec. VI.

VIII. CONCLUSION

Computer experiments on the dynamics of condensed matter systems show a complex structure of the phase space in the region of the transition from chaotic to ordered behavior. The results of Sec. III locate (in the energy range) the transition region for 2D and 3D square lattices, and provide insight into its dynamics, characterized by the coexistence of ordered and chaotic patterns. This coexistence leads to a pronounced asymmetry in the behavior of different DOF's, clearly visible in their energy exchange regime. The use of nongeneric initial conditions, where only a few DOF's are excited, reveals a difference in the dynamical behavior of different DOF's which extends from a region of weak chaos into a region of strong chaos, where a global chaoticity—due to the presence of some chaotic DOF's—may hide the existence of other ordered DOF's.

The results shown in Sec. III stress the need for a new diagnostic tool suitable to give a measure of chaos and order of the single DOF's. This tool—while being easily computable and stable—has to be of pratical use for systems with many DOF's, and at the same time allow a detailed characterization of single DOF's and a synoptic view of the dynamical behavior of the whole system.

In Sec. IV we defined coherence angles through a geometrical analysis that relates the dynamical behavior of a DOF with its angular proximity to the most expanding direction in the tangent space of the phase space of the system. In Sec. V we showed that a small angle characterizes the most chaotic DOF's, while more ordered DOF's have directions well apart from the one characterized by the highest Lyapunov exponent. CA's were defined and measured as asymptotic quantities; on the other hand, the short and medium time dynamical behavior of the system is influenced by all the Lyapunov directions (expanding and contracting). To take into account this broader set of factors affecting the evolution of each DOF, in Sec. VI we generalized the definition of coherence angles. It turns out that there exists a particular disposition of the expanding and contracting Lyapunov vectors which could result to be a generic property of condensed matter systems. As a consequence of this disposition, CA's deliver most of the information which could be obtained—with a much heavier computational burden—by explicitly computing the generalized coherence angles between each DOF and all Lyapunov directions.

The information provided by the DOF's for the square lattices studied here shows that in the transition region different DOF's may have quite different degrees of chaos. This is an important problem, not only from a theoretical point of view, but also for the reliability of numerical simulations. When simulating equilibrium properties of a real system, one should ascertain that the simulated system is endowed with the required equilibrium dynamical properties. In molecular dynamics computer experiments, equilibrium time averages are assumed to be equivalent to ensemble averages. This is true if all DOF's behave chaotically, and in a similar way: this secures that the results are statistically meaningful, and do not depend on the initial state of the simulation.

However, an underlying ordered dynamics may cause troubles when measuring standard properties of standard model systems. As an example, one can take the specific heat at a constant volume of a Lennard-Jones crystal, measured in a system at constant energy through the fluctuation of the kinetic energy [22]. This quantity shows an absurd behavior at low temperature (positive and negative divergence), when computed over typical average times, which are usually sufficient to compute this same correctly quantity at higher temperatures. This happens because, due to the increase of order in the low energy dynamics, the fluctuation of the kinetic energy relaxes to its expected value over times which may be more than two orders of magnitude longer than the tipical ones [23,24]. How can one be sure that the system at hand is ''statistically correct,'' that is, that time averages are equivalent to ensemble averages? One obvious requirement is that the averages be computed over times which are significantly greater than the time needed by the most ordered DOF's to relax to equilibrium (which may become impossible at low energies).

In order to obtain a physically meaningful quantity, in Sec. VII we introduced *coherence times*, which give a measure of the time each DOF needs to relax to equilibrium. Our tools have been used to analyze the dynamics of simple microcrystals, as an example of Hamiltonian systems with many DOF's. Results for 2D and 3D Lennard-Jones lattices show that at high temperature all DOF's tend to the same level of chaoticity. On the other hand, at low temperature we found a nontrivial structure of the spectrum of CA's and of coherence times, indicating the coexistence of DOF's endowed with quite different degrees of chaoticity; and the relaxation times of the various DOF's seem to increase roughly with the inverse power of the specific energy e.

We will apply the diagnostic tools described in this paper to other condensed matter systems, e.g., molecules, to analyze their dynamics. A relevant question will be the spectrum of coherence times, and its dependence on the specific energy. We believe that the main features of the transition region found in the 2D and 3D square lattices are quite generic for condensed matter systems at low energy. On the other hand, the spectrum of the coherence times may well exhibit features which are specific to each system.

APPENDIX A

An intuitive explanation of the instability can be obtained as follows. Expanding K_T and K_L to first order in $d-r_0$, one finds that $(\omega^x_{1,N})^2=(\omega^y_{N,1})^2\leqslant 0$ when

$$\frac{r_0-d}{r_0}\geqslant \tan^2\frac{\pi}{2(N+1)}. \tag{A1}$$

These two are the first frequencies which become imaginary. For $N=8$ the maximum compression allowed before the lattice becomes unstable corresponds to $d\simeq r_0-0.03r_0$.

Looking at the displacements of the particles induced by the two modes of frequency $\omega^x_{1,N}$and $\omega^y_{N,1}$, for $N=8$ one derives:

$$u^x_{ij}=\frac{2}{9}(-1)^{j+1}q^x_{18}(t)\sin\frac{\pi i}{9}\sin\frac{\pi j}{9}, \tag{A2}$$

$$u^y_{ij}=\frac{2}{9}(-1)^{i+1}q^y_{81}(t)\sin\frac{\pi i}{9}\sin\frac{\pi j}{9}. \tag{A3}$$

Along each horizontal or vertical row, particles have longitudinal displacements of the same sign, and transversal displacements of alternate sign. Alternate rows have longitudinal displacements of opposite sign, and therefore tend to slip with respect to each other. This instability is due to the interaction being limited to the first neighbors, and is hindered by the fixed particles of the boundaries. Therefore, the maximum allowed compression diminishes when the size of the system increases, as shown by formula (A1).

In general one can write

$$u_{ij}(t)=\frac{2}{N+1}\sum_{hk} q_{hk}(t)\sin\left(\frac{h\pi i}{N+1}\right)\sin\left(\frac{k\pi j}{N+1}\right),$$

where

$$q_{hk}(t)\simeq A_{hk}\mathrm{Re}\exp[i(\omega_{hk}t+\varphi_{hk})].$$

If $\omega_{hk}\in \mathrm{Re}$,

$$\frac{1}{T}\int_0^T u_{ij}(t)dt=0 \quad \text{because} \quad \frac{1}{T}\int_0^T q_{hk}(t)dt=0.$$

If $\omega_{hk}\in \mathrm{Im}$,

$$\frac{1}{T}\int_0^T u_{ij}(t)dt\neq 0 \quad \text{because} \quad \frac{1}{T}\int_0^T q_{hk}(t)dt\neq 0.$$

In the first case the particles oscillate around their stable equilibrium position. In the second case they do not remain around their (nonstable) position, but move to a new stable position.

APPENDIX B

In this appendix we give a description of the modified central difference algorithm we have used in our numerical simulations. If $\mathbf{r}$, $\mathbf{v}$, and M are the position, velocity, and mass of a generic particle, respectively, $\mathbf{F}$ the force acting on it, and h the time step in the integration of the equations of motion, then

$$\mathbf{r}(t\pm h)=\mathbf{r}(t)\pm h\mathbf{v}(t)+\frac{h^2}{2M}\mathbf{F}(t)\pm\frac{h^3}{6M}\dot{\mathbf{F}}(t)+O(h^4). \tag{B1}$$

The standard central difference algorithm is obtained summing and subtracting the two equations (B1), obtaining:

$$\mathbf{r}(t+h)=-\mathbf{r}(t-h)+2\mathbf{r}(t)+\frac{h^2}{M}\mathbf{F}(t)+O(h^4),$$

$$\mathbf{v}(t)=\frac{\mathbf{r}(t+h)-\mathbf{r}(t-h)}{2h}+O(h^2). \tag{B2}$$

With such an algorithm the velocities are known with a precision lower by two orders of magnitude in the time step than that of the positions: this is not a problem for the dynamical evolution of the system, but it may affect the computation of thermodynamical quantities.

To improve by one order the precision in the velocities, instead of Eqs. (B2) we used

$$\mathbf{r}(t\pm h)=\mathbf{r}(t)\pm h\mathbf{v}(t)+\frac{h^2}{2M}\mathbf{F}(t)\pm\frac{h^3}{6M}\dot{\mathbf{F}}(t)+O(h^4),$$

$$h\mathbf{v}(t-h)=h\mathbf{v}(t)-\frac{h^2}{M}\mathbf{F}(t)+\frac{h^3}{2M}\dot{\mathbf{F}}(t)+O(h^4).$$

Combining these equations we obtain

$$\mathbf{v}(t)=\frac{1}{h}\left[\frac{3}{2}(\mathbf{r}(t)-\mathbf{r}(t-h))-\frac{1}{2}h\mathbf{v}(t-h)+\frac{h^2}{4M}\mathbf{F}(t)\right]+O(h^3)$$

The improvement in the computation of the velocities, and thus of the kinetic energy, enhances the conservation of the total energy during the time evolution of the system.

APPENDIX C

The explicit calculation of the equations of motion in the tangent space of a Lennard-Jones lattice is rather cumbersome. Here we give only the final equations for the 2D and 3D lattices, also in order to show the numerical burden that the tangent dynamics introduces in the simulation. For the 2D lattice we have

$$\delta\ddot{x}_{lm}(t)=\sum_{l,'m'}\left\{\left[\left(V''-\frac{V'}{r}\right)\left(\frac{\tilde{x}(t)}{r}\right)^2+\frac{V'}{r}\right]\delta\tilde{x}(t)+\left(V''-\frac{V'}{r}\right)\frac{\tilde{x}(t)}{r}\frac{\tilde{y}(t)}{r}\delta\tilde{y}(t)\right\},$$

$$\delta\ddot{y}_{lm}(t)=\sum_{l',m'}\left\{\left[\left(V''-\frac{V'}{r}\right)\left(\frac{\tilde{y}(t)}{r}\right)^2+\frac{V'}{r}\right]\delta\tilde{y}(t)+\left(V''-\frac{V'}{r}\right)\frac{\tilde{y}(t)}{r}\frac{\tilde{x}(t)}{r}\delta\tilde{x}(t)\right\},$$

where $V'=dV/dr$, $V''=d^2V/dr^2$ [V is the Lennard-Jones potential of formula (1)], and the sum is over all the particles. (l,m) are the indices of a particle, $\delta x_{lm}(t)$ and $\delta y_{lm}(t)$ are the tangent coordinates of particle (l,m); $\tilde{x}=x_{lm}-x_{l'm'}$, $\tilde{y}=y_{lm}-y_{l'm'}$, and r is the distance of particle (l,m) from particle (l',m'); $\delta\tilde{x}=\delta x_{lm}-\delta x_{l'm'}$ and $\delta\tilde{y}=\delta y_{lm}-\delta y_{l'm'}$.

In three dimensions the equations are

$$\delta\ddot{x}_{lmn}(t)=\sum_{l,'m,'n'}\left\{\left[\left(V''-\frac{V'}{r}\right)\left(\frac{\tilde{x}(t)}{r}\right)^2+\frac{V'}{r}\right]\delta\tilde{x}(t)+\left(V''-\frac{V'}{r}\right)\frac{\tilde{x}(t)}{r}\left[\frac{\tilde{y}(t)}{r}\delta\tilde{y}(t)+\frac{\tilde{z}(t)}{r}\delta\tilde{z}(t)\right]\right\},$$

$$\delta\ddot{y}_{lmn}(t)=\sum_{l',m',n'}\left\{\left[\left(V''-\frac{V'}{r}\right)\left(\frac{\tilde{y}(t)}{r}\right)^2+\frac{V'}{r}\right]\delta\tilde{y}(t)+\left(V''-\frac{V'}{r}\right)\frac{\tilde{y}(t)}{r}\left[\frac{\tilde{x}(t)}{r}\delta\tilde{x}(t)+\frac{\tilde{z}(t)}{r}\delta\tilde{z}(t)\right]\right\},$$

$$\delta\ddot{z}_{lmn}(t)=\sum_{l',m',n'}\left\{\left[\left(V''-\frac{V'}{r}\right)\left(\frac{\tilde{z}(t)}{r}\right)^2+\frac{V'}{r}\right]\delta\tilde{z}(t)+\left(V''-\frac{V'}{r}\right)\frac{\tilde{z}(t)}{r}\left[\frac{\tilde{x}(t)}{r}\delta\tilde{x}(t)+\frac{\tilde{y}(t)}{r}\delta\tilde{y}(t)\right]\right\}.$$

APPENDIX D

For the sake of simplicity we restrict our discussion to a nondegenerate Lyapunov spectrum, so that each vector $\hat{\mathbf{e}}_i$ corresponds to a different λ_i; the extension to the case of degeneracy is straightforward. Let us decompose each vector of the set $\{\hat{\mathbf{e}}_i\}$ $(i>1)$ into two components, one parallel and one orthogonal to $\hat{\mathbf{e}}_1$ (the maximum expansion direction): $\hat{\mathbf{e}}_i \equiv \mathbf{e}_{i,p}+\mathbf{e}_{i,o}$, $i=2,\ldots,m$ with $\mathbf{e}_{i,p}\equiv(\mathbf{e}_1\cdot\mathbf{e}_i)\hat{\mathbf{e}}_1$ and $\mathbf{e}_{i,o}\equiv\hat{\mathbf{e}}_i-\mathbf{e}_{i,p}$.

Let us write the tangent vector $\mathbf{w}(t)$ using this decomposition:

$$\begin{aligned}\mathbf{w}(t) &= c_1(t)\exp(\lambda_1 t)\hat{\mathbf{e}}_1+\sum_{k=2}^{m}c_k(t)\exp(\lambda_k t)(\mathbf{e}_{k,p}+\mathbf{e}_{k,o})= \\ &= \hat{\mathbf{e}}_1\underbrace{\left[c_1(t)\exp(\lambda_1 t)+\sum_{k=2}^{m}c_k\exp(\lambda_k t)(\hat{\mathbf{e}}_1\cdot\mathbf{e}_k)\right]}_{a_1}+\sum_{k=2}^{m}\mathbf{e}_{k,o}\underbrace{c_k\exp(\lambda_k t)}_{a_k}= \\ &= \sum_{k=1}^{m}a_k\mathbf{v}_k\ ,\end{aligned}$$

where

$$\lim_{t\to\infty}\frac{1}{t}\ln a_1=\lim_{t\to\infty}\frac{1}{t}\ln c_1\exp(\lambda_1 t)=\lim_{t\to\infty}\frac{1}{t}\ln c_1+\lambda_1=\lambda_1,$$

$$\lim_{t\to\infty}\frac{1}{t}\ln a_k=\lambda_k,\quad k=2,\ldots,m$$

and

$$\mathbf{v}_1=\hat{\mathbf{e}}_1,$$

$$\mathbf{v}_k=\mathbf{e}_{k,o},\quad k=2,\ldots,m.$$

Each $\mathbf{v}_k$ $(k>1)$ is orthogonal to $\hat{\mathbf{e}}_1$.

The coefficient a_2 of $\mathbf{v}_2$ grows asymptotically like $\exp(\lambda_2 t)$. We can now decompose each $\mathbf{v}_k$ $(k>2)$ into two components, one parallel and one orthogonal to $\mathbf{v}_2$.

Iterating this method for each $\mathbf{v}_k$ we obtain $\mathbf{w}(t)=\sum_{k=1}^{m}\tilde{a}_k\tilde{\mathbf{v}}_k$, where

$$\tilde{\mathbf{v}}_1=\hat{\mathbf{e}}_1,$$

$$\tilde{\mathbf{v}}_2=\hat{\mathbf{e}}_2-\frac{\tilde{\mathbf{v}}_1\cdot\hat{\mathbf{e}}_2}{\tilde{\mathbf{v}}_1\cdot\tilde{\mathbf{v}}_1}\tilde{\mathbf{v}}_1,$$

$$\tilde{\mathbf{v}}_3=\hat{\mathbf{e}}_3-\frac{\tilde{\mathbf{v}}_1\cdot\hat{\mathbf{e}}_3}{\tilde{\mathbf{v}}_1\cdot\tilde{\mathbf{v}}_1}\tilde{\mathbf{v}}_1-\frac{\tilde{\mathbf{v}}_2\cdot\hat{\mathbf{e}}_3}{\tilde{\mathbf{v}}_2\cdot\tilde{\mathbf{v}}_2}\tilde{\mathbf{v}}_2,$$

$$\tilde{\mathbf{v}}_4=\hat{\mathbf{e}}_4-\frac{\tilde{\mathbf{v}}_1\cdot\hat{\mathbf{e}}_4}{\tilde{\mathbf{v}}_1\cdot\tilde{\mathbf{v}}_1}\tilde{\mathbf{v}}_1-\frac{\tilde{\mathbf{v}}_2\cdot\hat{\mathbf{e}}_4}{\tilde{\mathbf{v}}_2\cdot\tilde{\mathbf{v}}_2}\tilde{\mathbf{v}}_2-\frac{\tilde{\mathbf{v}}_3\cdot\hat{\mathbf{e}}_4}{\tilde{\mathbf{v}}_3\cdot\tilde{\mathbf{v}}_3}\tilde{\mathbf{v}}_3,$$

$$\ldots \quad \ldots,$$

$$\ldots \quad \ldots,$$

and $\lim_{t\to\infty}(1/t)\ln\tilde{a}_k=\lambda_k\ \forall\ k$, each $\tilde{a}_k$ being a linear combination of $\exp(\lambda_i t)$ $(i\geqslant k)$. In this way we have constructed a set of *orthogonal* vectors $\{\tilde{\mathbf{v}}_k\}$ in each tangent space $T\Re_{\mathbf{x}(t)}$; the vectors evolve asymptotically with rates given by the set of Lyapunov exponents $\{\lambda_i\}$.

[1] H. Poincaré, *Les Méthodes Nouvelles de la Méchanique Celeste* (Blanchard, Paris, 1987), Vol. 3, p. 398.

[2] E. Fermi, Nuovo Cimento **25**, 267 (1923); **26**, 105 (1923).

[3] E. Fermi, J.R. Pasta, and S. Ulam, *Collected Works of Enrico Fermi* (University of Chicago Press, Chicago, 1965), Vol. 2, p. 978.

[4] A.N. Kolmogorov, Dokl. Acad. Nauk. SSSR **98**, 527 (1954). J. Moser, Nachr. Akad. Wiss. Goett. II, Math.-Phys. Kl. **1**, 1 (1962); V.I. Arnold, Russian Mathematical Survey **18**, 9 (1963).

[5] M. Pettini and M. Landolfi, Phys. Rev. A **41**, 768 (1990).

[6] L. Galgani, Scientia (Milan) **110**, 469 (1975).

[7] N.N. Nekhoroshev, Transactions Moscow Mathematical Society **32**, 1 (1977).

[8] M. Pettini and M. Cerruti-Sola, Phys. Rev. A **44**, 975 (1991).

[9] L. Boltzmann, Nature (London) **51**, 413 (1895).

[10] G. Benettin, G. Lo Vecchio, and A. Tenenbaum, Phys. Rev. A **22**, 1709 (1980).

[11] G. Benettin and A. Tenenbaum, Phys. Rev. A **28**, 3020 (1983).

[12] M. D'Alessandro and A. Tenenbaum, Phys. Rev. E **52**, R2141 (1995).

[13] A. Campa, A. Giansanti, and A. Tenenbaum, J. Phys. A **25**, 1915 (1992).

[14] M. D'Alessandro, A. D'Aquino, and A. Tenenbaum, Physica A **240**, 115 (1997).

[15] The reduced Lennard-Jones units are σ for the length, ϵ for the energy, and $\tau=(M\sigma^2/48\epsilon)^{1/2}$ for the time. The values of these parameters appropriate for argon are $\sigma=3.405$ Å; $\epsilon=119.8k_B$, and $\tau=3.112\times10^{-13}$ s.

[16] V. I. Osedelec, Trans. Moscow Math. Soc. **19**, 197 (1968).

[17] G. Benettin, L. Galgani, and J. M. Strelcyn, Phys. Rev. A **14**, 2338 (1976).

[18] G. Benettin, L. Galgani, and A. Giorgilli, Phys. Lett. A **120**, 23 (1987).

[19] G. Benettin, L. Galgani, and A. Giorgilli, Nature (London) **311**, 444 (1984).

[20] H. Posch and W. Hoover, Phys. Rev. A **39**, 2175 (1989).

[21] I. Borzsák, H. A. Posch, and A. Baranyai, Phys. Rev. E **53**, 3694 (1996).

[22] J. L. Lebowitz, J. K. Percus, and L. Verlet, Phys. Rev. **153**, 250 (1967).

[23] R. Simonazzi and A. Tenenbaum, Phys. Rev. E **54**, 964 (1996).

[24] A. Perronace and A. Tenenbaum, Phys. Rev. E **57**, 100 (1998).